APPLIED PHYSICS

Basis function approach for diffractive pattern generation with Dammann vortex metasurfaces

Xue Zhang[1], Lingling Huang[1]*, Ruizhe Zhao[1], Hongqiang Zhou[1], Xin Li[1], Guangzhou Geng[2], Junjie Li[2], Xiaowei Li[3], Yongtian Wang[1]*, Shuang Zhang[4,5]*

In mathematics, general functions can be decomposed into a linear combination of basis functions. This principle can be used for creating an infinite number of distinct geometric patterns based on a finite number of basis patterns. Here, we propose a Dammann vortex metasurface (DVM) for optically generating an array of diverse, diffraction-multiplexed vortex patterns, based on three custom-defined basis patterns. The proposed DVM, with its capability of quantitatively correlating phase and intensity distribution in different diffraction orders, opens up doors for various applications including orbital angular momentum encryptions and quantum entanglement.

INTRODUCTION

All-optical computing represents a powerful means for handling abundant data analysis workloads with fast process abilities, which may go beyond the conventional electronic chip method (*1*–*3*). Specifically, optical devices can be used to perform mathematical operations and information processing through wavefront engineering. For example, lenses are excellent operators for Fourier transformation, and previously reported optical elements can also be designed to achieve edge detection through differentiation (*4*–*6*), integration, transformation of structured light carrying orbital angular momentum (OAM) (*7*–*10*), etc. Basis functions are widely used in mathematics, which play key roles in interpreting complex functions, and serve as an extremely powerful tool for universal computing in algebra and other related fields such as communications (*11*–*13*). However, building optical architectures based on the concept of basis functions has been rarely explored.

Metasurfaces, ultrathin structured surfaces for manipulating the wavefront of light, feature unlimited optical modulation abilities benefitting from the well-tailored optical response of individual meta-atoms in the nanometer scale (*14*–*19*). Metasurfaces can be designed to manipulate the polarization, phase, and amplitude of transmitted or reflected beam. Because of their subwavelength pixel size, metasurfaces are more suitable for applications that require large numerical aperture (diffraction angle) than traditional spatial light modulators (SLMs) and diffractive optical elements (*20*, *21*). In addition, metasurfaces provide complicated and accurate control of the optical beams. Geometric phase is widely applied in the design of metasurfaces (*14*, *22*, *23*), which arises from the conversion between beams of different circular polarization states and exhibits dispersionless property (*24*). Such phase can be easily encoded into the orientations of meta-atoms, which can ease the design process. Various applications based on metasurfaces have been proposed and demonstrated, such as holography (*23*, *25*, *26*), vectorial optics (*27*–*33*), structural beam generation (*34*–*36*), beam shaping (*37*), and optical information multiplexing (*12*, *38*, *39*). For example, metasurface has been demonstrated for generating vortex arrays with donut intensity profiles (*40*). Similar to diffractive optics framework for machine learning (*1*), metasurfaces may show great potential in all-optical computation for object classification and imaging and for other task-specific optical manipulations.

Here, we propose and demonstrate a previously unexplored approach for diffraction-multiplexed generation of generalized vortex beams (GVBs) based on the linear combination of a few custom-defined basis patterns, by using Dammann vortex metasurface (DVM). As shown previously (*41*), GVBs have a custom-defined angular phase distribution, i.e., the local angular phase gradient is no longer a constant like the conventional vortex beams. The angular phase distribution directly controls the intensity profiles of the vortex beams. On the basis of this design approach, we experimentally demonstrate several examples of DVMs with diffraction-multiplexed patterns by using three custom-defined basis patterns. Realization of pattern generation in different diffraction orders may provide unique opportunities for optical computing in terms of parallelization, scalability, and fast computational speed.

RESULTS

Figure 1 schematically shows the generation of diffraction-multiplexed GVB array based on a dielectric geometric DVM. The spatial feature of each diffraction order is no longer that of a conventional vortex beam of donut shape but exhibits diverse intensity profiles carrying OAM. The azimuthal phase profile of each of the diffraction orders can be obtained through Taylor series expansion of vortex grating function. Specifically, different configurations of GVBs are generated in different diffraction orders, and the field patterns represent the linear combinations of preset basis functions (Fig. 1A) encoded on the DVM. Such phenomenon can be applied in various fields, such as optical representation of mathematical computation, optical communication based on OAM multiplexing and demultiplexing, optical information processing, and particle manipulation. In the following, we explain the design principle in detail.

Design principle of DVM

The global topological charge L_0 of a GVB can be expressed as the integral of the phase gradient along the azimuth angle

[1]Beijing Engineering Research Center of Mixed Reality and Advanced Display, School of Optics and Photonics, Beijing Institute of Technology, Beijing 100081, China. [2]Beijing National Laboratory for Condensed Matter Physics, Institute of Physics, Chinese Academy of Sciences, Beijing 100191, China. [3]Laser Micro/Nano-Fabrication Laboratory, School of Mechanical Engineering, Beijing Institute of Technology, Beijing 100081, China. [4]Department of Physics, University of Hong Kong, Hong Kong, China. [5]Department of Electrical and Electronic Engineering, University of Hong Kong, Hong Kong, China.
*Corresponding author. Email: huanglingling@bit.edu.cn (L.H.); wyt@bit.edu.cn (Y.W.); shuzhang@hku.hk (S.Z.)

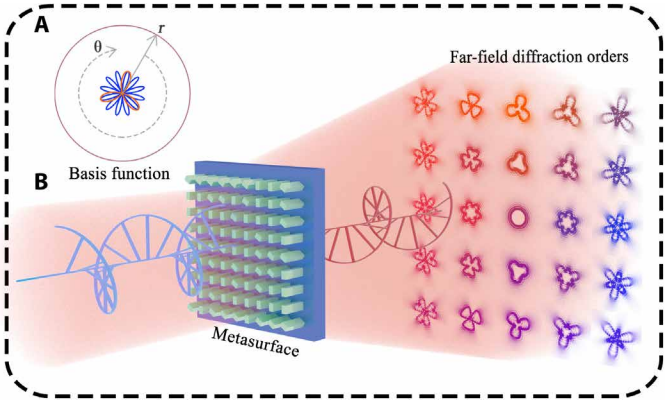

Fig. 1. Scheme of DVM based on dielectric geometric metasurface. (**A**) Diffraction channels (5 × 5) with different intensity patterns of GVBs under orthogonal circular polarization input and output condition. (**B**) The basis function curves of differential adder and subtractor.

$$\int_0^{2\pi} \frac{d\varphi(\theta)}{d\theta} d\theta = 2\pi L_0 \quad (1)$$

where $d\varphi(\theta)/d\theta$ is the local azimuthal phase gradient, which is generally not a constant for the GVB. Thus, the complex amplitude of the GVB can be expressed as $e^{i\varphi(\theta)}$. For GVB, the radius R of beam intensity profile in k space is proportional to the phase gradient as $R(\theta_k) \propto \frac{d\varphi(\theta)}{d\theta}$ with $\theta_k = \theta + \pi/2$, which determines the intensity profile (*41*).

DVMs with phase-only modulation are designed to generate the desired intensity profiles of GVBs for different diffraction orders. Each superperiod consists of several pixel arrays in the form of a fork-like chessboard with optimized phase distributions. Such DVM can realize multiplexing/demultiplexing by generating/detecting the spatial distribution of OAMs within the target diffraction orders. The checkerboard-shaped grating period distribution is superimposed by the phase distribution of the vortex beam. Different vortex information can be obtained for each diffraction order. The overall transmission function of DVM is expressed as

$$T_{\mathrm{DVM}} = \exp(i\varphi_0) \sum_{m=-\infty}^{+\infty} \sum_{n=-\infty}^{+\infty} C_{mn} \exp\left(i \left[\frac{2\pi m x}{T_x} + \frac{2\pi n y}{T_y} + m\varphi_x + n\varphi_y \right] \right) \quad (2)$$

where T_{DVM} represents the complex transmission coefficient feature of the DVM, which can be expanded into different diffraction orders of (m, n). φ_0, φ_x, and φ_y serve as three basis functions, whose linear combinations lead to different GVBs at different diffraction orders, i.e., the phase profile in diffraction order (m, n) can be expressed as $\varphi_0 + m\varphi_x + n\varphi_y$. T_x and T_y are the period along x and y directions. For each super lattice period, $T_x = \mathrm{Num}_x \cdot p$ and $T_y = \mathrm{Num}_y \cdot p$, where p represents the lattice constant, and $\mathrm{Num}_x \times \mathrm{Num}_y$ is the total number of pixels within each superperiod. For phase-type Dammann grating, the amplitude A_0 is constant, and C_{mn} represents the amplitude of each diffraction order. In our design, uniform C_{mn} values are achieved for the target diffraction orders, with relatively high total efficiency and suppressed undesired orders.

To verify the working principle of DVM, first, we choose the number of diffraction orders along each direction as $M = 3$, $N = 3$, that is, m and n can be 0 and ±1. The phase-type Dammann grating

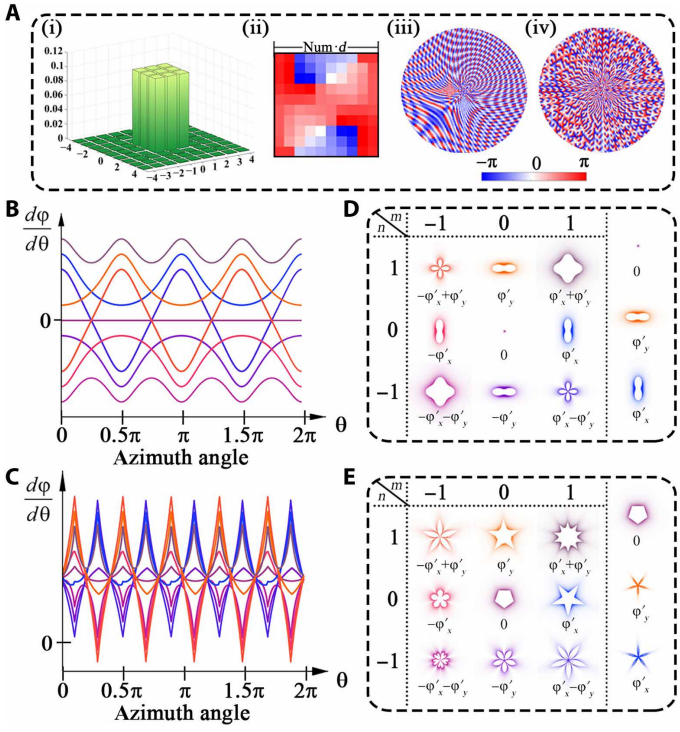

Fig. 2. Working principle of DVM based on the Dammann optimization method. (**A**) Details of Dammann optimization. (i) Intensity distribution of 3 × 3 optimized diffraction orders. (ii) Optimized phase of one superperiod. (iii and iv) Distribution of the whole DVM with the filled optimized phase for samples 1 and 2. (**B** and **C**) Local phase gradient versus azimuthal angle for the nine diffraction orders by obeying the law of $\varphi_0 + m\varphi_x + n\varphi_y$. (**D** and **E**) Various intensity patterns of each GVB in each diffraction channel of DVM.

diffracts an incident beam into the desired intensity distribution of the target diffraction orders through the optimization of the phase distribution within a superperiod. One can define the loss function for evaluation with the criterion that the target diffraction orders have the maximum and equal intensity. The pixel number of each superperiod is chosen as Num = 10. For target diffraction orders $M \times N$, the optimized transmission coefficient is $C_{mn} = \frac{1}{\sqrt{M \times N}}$, and the corresponding intensity proportion is $I_{mn} = \frac{1}{M \times N}$. Adopting genetic algorithm, the optimal intensity distribution can be obtained through varying the phase within the superperiod, as shown in Fig. 2A (i), and the corresponding phase distribution is shown in Fig. 2A (ii). The optimized I_{mn} values of target orders are all more than 10% with almost uniform distribution and those of the unwanted diffraction orders are all less than 1%, as shown in Fig. 2A (i). In each of the net-like periodic zones, the optimized Dammann phase distribution can be imprinted onto the corresponding pixel of DVM, with the final integrated phase (x, y) shown in Fig. 2A (iii and iv).

Two DVMs (samples 1 and 2) with different sets of basic functions φ_0, φ_x, and φ_y are designed, as shown in Fig. 2. The phase gradients of different diffraction orders along the azimuthal direction are represented by curves of different colors in Fig. 2 (B and C). The resulting intensity patterns of GVBs in the nine diffraction orders with the combination of $m = -1, 0, 1$ and $n = -1, 0, 1$ are shown in Fig. 2 (D and E). The intensity profiles corresponding to the basis functions are given on the right side. The phase distributions of the diffraction

orders, satisfying $\varphi_{m,n}(\theta) = \varphi_0 + m\varphi_x + n\varphi_y$, lead to completely different intensity patterns. For sample 1 (Fig. 2D), we have $\varphi_0 = 0$, and the intensity profile of φ_x and φ_y has a peanut shape expressed as $\frac{d\varphi_x(\theta)}{d\theta} = \frac{70}{\sin^2\theta + 3\cos^2\theta} + 8$ and $\varphi_y(\theta) = \varphi_x(\theta + \pi/2)$, leading to centrosymmetric distributions of different diffraction orders about the center. For sample 2, φ_0 is a basis function corresponding to a pentagon shape, while φ_x and φ_y are correlated as $\varphi_y(\theta) = 1.1 \cdot \varphi_x(\theta - \pi/5)$. Here, φ_x is designed to combine with φ_0 to produce a normal star-like shape in (0,1) order. The intensity feature of all the nine diffraction orders is different in this case, and the centrosymmetry is broken, as illustrated in Fig. 2 (D and E). More details about the analytic approach of GVB can be seen in section S1 for (0,0) order of sample 2 as an example. The design details of the Si antenna for DVM fabrication can be found in the Supplementary Materials (fig. S2).

We further design a 5 × 5 Dammann metasurface (sample 3) with the three basis phase functions $\varphi_0 = 30\theta$, $\varphi_x = -\frac{5}{3}\cos(6\theta)$, and $\varphi_y = -\frac{10}{3}\cos\left(3\theta + \frac{\pi}{4}\right)$, and the diffraction features are shown in Fig. 3. For each diffraction order, the different linear combinations of φ_0, φ_x, and φ_y can result in different beam shapes. The corresponding GVB intensity profiles determined by φ'_0, φ'_x, and φ'_y (where $'$ denotes the differential) appear as petals around the center, as shown in Fig. 3C (i to iv). On the basis of the diffraction law of such Dammann metasurface, the intensity profile of each diffraction order of the grating can be expressed as

$$R(\theta_k) \propto \frac{d\varphi}{d\theta} = 30 + 10m \times \sin(6\theta) + 10n \times \sin(3\theta + \pi/4) \quad (3)$$

Similarly, we design another Dammann metasurface (sample 4) with 7 × 7 diffraction orders by using another set of trigonometric functions $\varphi_0 = 30\theta$, $\varphi_x = -3\cos(2\theta)$, and $\varphi_y = -2\cos(3\theta - \pi/4)$, with the corresponding intensity profiles expressed as

$$R(\theta_k) \propto \frac{d\varphi}{d\theta} = 30 + 6m \times \sin(2\theta) + 6n \times \sin(3\theta - \pi/4) \quad (4)$$

All the design processes and the simulation of intensity patterns in the Fourier plane can be found in the Supplementary Materials (fig. S3).

Experimental demonstration

Following the DVM design methods, we fabricate the metasurfaces as shown in fig. S2. The height of the Si antennas and the pitch of the array for all samples are fixed as H = 600 nm and P = 500 nm, respectively. The diameter of the metasurface is 400 μm. The length L and the width W of the rectangle antennas are L = 195 nm and W = 125 nm. We encode the desired phase profiles into the metasurface based on the geometric phase principle. The experimental setup of geometric metasurface is shown in Fig. 4A. The top view and side view of the scanning electron microscopy (SEM) images are shown in Fig. 4 (B and C). More details about the design and fabrication of dielectric metasurface can be seen in section S2.

In the experiment, a Fourier lens and a charge-coupled device (CCD) camera are used to capture the beam profile of the output light at the Fourier plane. We present the experiment results of DVM for the four samples at a working wavelength of 800 nm. Besides the observation of the target intensity patterns on the Fourier plane, we also investigate the spatial evolution of the GVB patterns at different locations away from the Fourier plane. In Fig. 5, the simulation and experiment results of samples 1 and 2 are shown in the range from −30 to 30 mm along the Z direction relative to the Fourier plane. The DVM's light field spatial evolution of samples 1 and 2 can be viewed in movies S1 and S2. The diffraction images are calculated via Fourier transform based on the designed phase distribution on the metasurfaces. At the Fourier plane ($\Delta z = 0$), the intensity profiles of both simulation and experiment results match well with that of the designed ones for all the diffraction orders. For the experimental results of sample 1, there is no pattern in the central order with $\varphi_0 = 0$, and the other orders show a symmetrical intensity profile around the center. For sample 2, we observed nine different

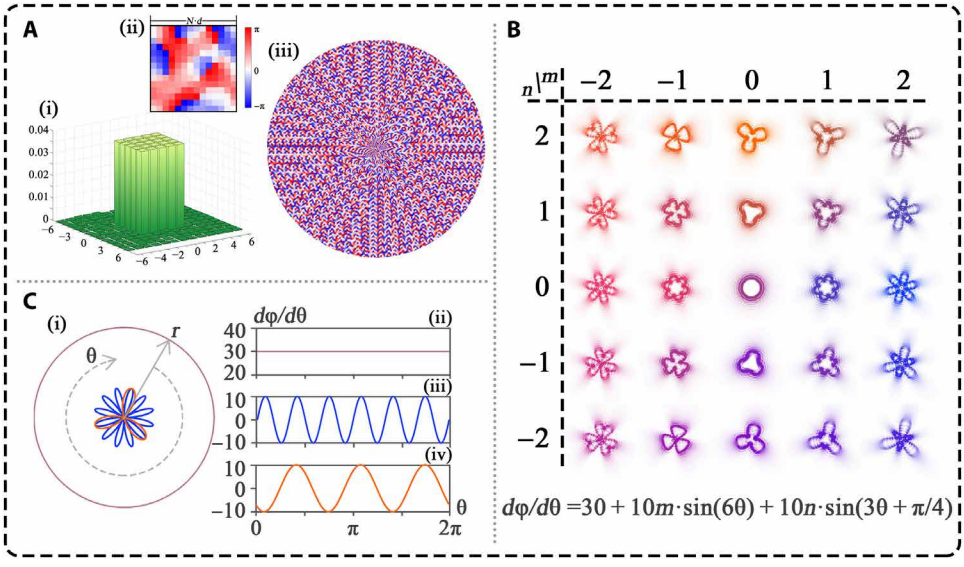

Fig. 3. Working principle of the special differential calculator based on DVM. (**A**) Details of Dammann optimization for sample 3. (i) Intensity distribution of 5 × 5 optimized diffraction orders. (ii) Optimized phase of one superperiod. (iii) Distribution of the whole DVM with the filled optimized phase for sample 3. (**B**) Various intensity patterns of each GVB in each diffraction channel of DVM. (**C**) (i to iv) Radius profile and differential function of three basic phase differential features φ'_0, φ'_x, and φ'_y in the polar coordinate and Cartesian coordinate.

GVB shapes. In addition, there is a bright zero-order spot in the center of sample 2, owing to the deviation of the fabricated patterns from the designed ones. The intensity profile of each diffraction order shows interesting twisting and/or deformation behaviors in the spatial evolution along the Z direction.

Similarly, for the other two samples (samples 3 and 4), all the desired patterns appear in the Fourier plane (with $Z = 0$), which represent the differential addition and subtraction of the trigonometric functions according to Eqs. 3 and 4 (the DVM's spatial evolution of samples 3 and 4 can be viewed in movies S3 and S4). We prove that all the intensity profiles agree well with the mathematical calculations based on the basis patterns (as shown in Fig. 6 and fig. S4). The method can be extended to larger arrays of diffraction orders with enhanced information capacity. Meanwhile, the metasurfaces show broadband operation, which is confirmed by additional measurement across a broad wavelength range between 700 and 860 nm (as shown in figs. S5 and S6). A more detailed analysis can be seen in section S3.

Meanwhile, such GVB beams can even have a vectorial feature by simultaneously modulating the phase and polarization properties of metasurfaces (as shown in fig. S7 and section S4). We further demonstrate that such DVM can operate on arbitrary incident GVB beam profiles. For an incident GVB with a given phase profile φ_{in}, in combination with the encoded phase on the DVM, the phase profile of the output-diffracted beams can be expressed with $\varphi_{out} = \varphi_{in} + \varphi_{DVM} = \varphi_{in} + \varphi_0 + m\varphi_x + n\varphi_y$. Hence, the shape of the contour of the GVB in the Fourier plane is given by the linear superpositions of the phase differential of $R_{\varphi_{in}}(\theta_k) \propto \frac{d\varphi_{in}}{d\theta} + \frac{d\varphi_0}{d\theta} + m\frac{d\varphi_x}{d\theta} + n\frac{d\varphi_y}{d\theta}$. That is, one can achieve addition and subtraction operations of the differentials of custom-defined incident functions within all the diffraction orders by parallel computation. Different input GVB beams with square, four-pointed star, five-pointed star, heart curve, and flash curve shapes are used as examples, and the corresponding differential operations in the form of intuitive intensity profiles are demonstrated (fig. S8). More details can be seen in section S5.

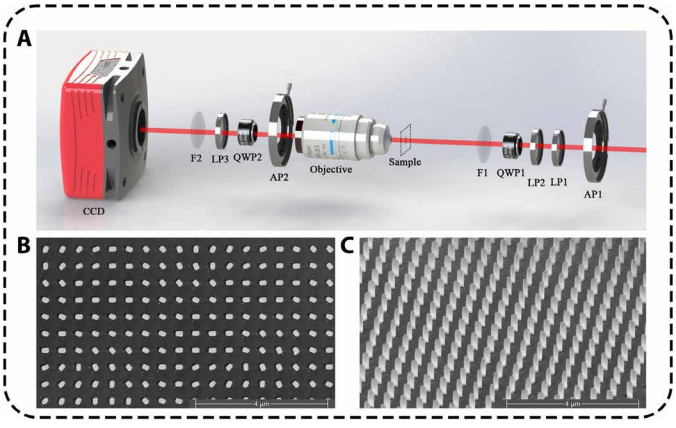

Fig. 4. Experiment setup and the SEM images of metasurface. (**A**) Optical setup for the observation of GVB in orthogonal circular polarization. AP, aperture; LP, linear polarizer; QWP, quarter–wave plate. (**B** and **C**) Top view and side view of SEM images of one fabricated silicon metasurface sample. The metasurface holograms are composed of 800 × 800 nanofins with the same size but different orientation angles.

DISCUSSION

In summary, we have proposed and demonstrated the generation of an array of GVBs using the linear combination of a set of basis functions enabled by metasurfaces. The Dammann optimization method is applied to achieve uniform intensity distributions among the target diffraction orders. Such DVM can generate a GVB array by using the phase relationship within each of the diffraction orders, which uses the flexibility of arbitrary angular phase differential design freedom. Hence, in different spatial diffraction orders, the generated GVB beams are different from each other, rather than donut shapes. It provides an optical representation of mathematical computation features. Such DVM may open doors for exploring various applications

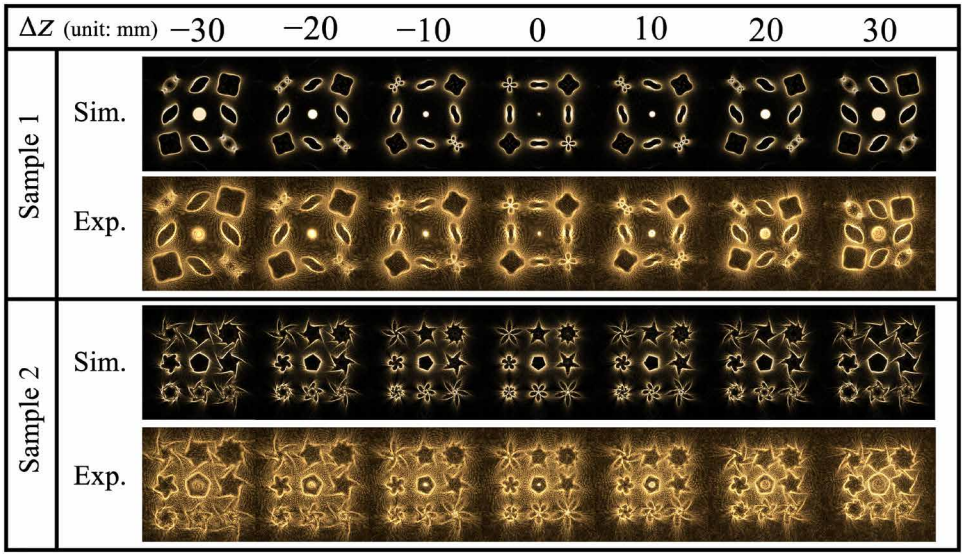

Fig. 5. Simulation and experiment results of spatial evolution on both sides of the Fourier plane of samples 1 and 2. The observation planes before and after the Fourier plane with a step size of 10 mm. The experiment results show good correspondence with the simulation ones.

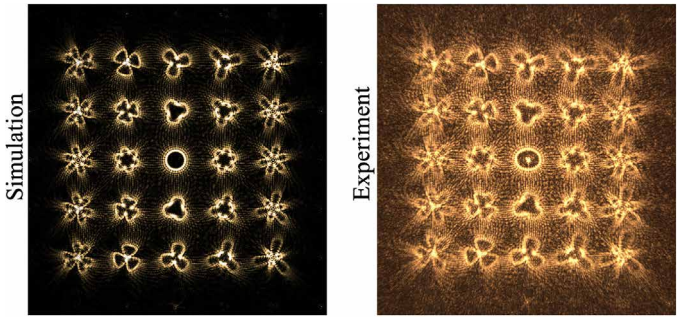

Fig. 6. Simulation and experimental results of the special differential calculator based on DVM in the Fourier plane of sample 3.

such as vortex information encryption, optical manipulation and optical communications, and quantum entanglement.

METHODS

The experimental setup

We use an experimental setup as shown in Fig. 4 to demonstrate the generation of DVM based on geometric metasurface. Supercontinuum laser is applied to provide a different coherent wavelength. The linear polarizers and quarter–wave plates are positioned in front of the sample to modulate the input and output polarization. Because of the submillimeter size of the reconstructed images, a 60× magnifying microscope objective, a Fourier lens, and a CCD are positioned behind the sample to capture the complex amplitude profile of the output light.

Measurement of conversion efficiency

To test the conversion efficiency of the circular polarization, we removed the CCD from the light path and replaced it with a power meter. We measured the optical power passing through the sample and the bare substrate under the cross-polarization condition. The conversion efficiency is defined as $\frac{|E_L|^2}{|E_R|^2+|E_L|^2}$. We showed the efficiency of the two circular polarizations for one sample in fig. S6.

SUPPLEMENTARY MATERIALS

Supplementary material for this article is available at https://science.org/doi/10.1126/sciadv.abp8073

REFERENCES AND NOTES

1. X. Lin, Y. Rivenson, N. T. Yardimci, M. Veli, Y. Luo, M. Jarrahi, A. Ozcan, All-optical machine learning using diffractive deep neural networks. *Science* **361**, 1004–1008 (2018).
2. A. Davies, P. Veličković, L. Buesing, S. Blackwell, D. Zheng, N. Tomašev, R. Tanburn, P. Battaglia, C. Blundell, A. Juhász, M. Lackenby, G. Williamson, D. Hassabis, P. Kohli, Advancing mathematics by guiding human intuition with AI. *Nature* **600**, 70–74 (2021).
3. G. Wetzstein, A. Ozcan, S. Gigan, S. Fan, D. Englund, M. Soljačić, C. Denz, D. A. B. Miller, D. Psaltis, Inference in artificial intelligence with deep optics and photonics. *Nature* **588**, 39–47 (2020).
4. T. Zhu, C. Guo, J. Huang, H. Wang, M. Orenstein, Z. Ruan, S. Fan, Topological optical differentiator. *Nat. Commun.* **12**, 680 (2021).
5. X. Qiu, F. Li, W. Zhang, Z. Zhu, L. Chen, Spiral phase contrast imaging in nonlinear optics: Seeing phase objects using invisible illumination. *Optica* **5**, 208 (2018).
6. P. Huo, C. Zhang, W. Zhu, M. Liu, S. Zhang, S. Zhang, L. Chen, H. J. Lezec, A. Agrawal, Y. Lu, T. Xu, Photonic spin-multiplexing metasurface for switchable spiral phase contrast imaging. *Nano Lett.* **20**, 2791–2798 (2020).
7. Y. Shen, X. Wang, Z. Xie, C. Min, X. Fu, Q. Liu, M. Gong, X. Yuan, Optical vortices 30 years on: OAM manipulation from topological charge to multiple singularities. *Light Sci. Appl.* **8**, 90 (2019).
8. A. Forbes, M. de Oliveira, M. R. Dennis, Structured light. *Nat. Photonics* **15**, 253–262 (2021).
9. A. H. Dorrah, N. A. Rubin, M. Tamagnone, A. Zaidi, F. Capasso, Structuring total angular momentum of light along the propagation direction with polarization-controlled meta-optics. *Nat. Commun.* **12**, 6249 (2021).
10. J. Xavier, S. Vyas, P. Senthilkumaran, J. Joseph, Complex 3D vortex lattice formation by phase-engineered multiple beam interference. *Int. J. Opt.* **2012**, 1–9 (2012).
11. J. Wang, J.-Y. Yang, I. M. Fazal, N. Ahmed, Y. Yan, H. Huang, Y. Ren, Y. Yue, S. Dolinar, M. Tur, A. E. Willner, Terabit free-space data transmission employing orbital angular momentum multiplexing. *Nat. Photonics* **6**, 488–496 (2012).
12. Z. H. Jiang, L. Kang, T. Yue, H. Xu, Y. Yang, Z. Jin, C. Yu, W. Hong, D. H. Werner, C. Qiu, A single noninterleaved metasurface for high-capacity and flexible mode multiplexing of higher-order Poincaré sphere beams. *Adv. Mater.* **32**, 1903983 (2020).
13. H. Ren, X. Fang, J. Jang, J. Bürger, J. Rho, S. A. Maier, Complex-amplitude metasurface-based orbital angular momentum holography in momentum space. *Nat. Nanotechnol.* **15**, 948–955 (2020).
14. N. Yu, P. Genevet, M. A. Kats, F. Aieta, J.-P. Tetienne, F. Capasso, Z. Gaburro, Light propagation with phase discontinuities: Generalized laws of reflection and refraction. *Science* **334**, 333–337 (2011).
15. L. Huang, X. Chen, H. Mühlenbernd, G. Li, B. Bai, Q. Tan, G. Jin, T. Zentgraf, S. Zhang, Dispersionless phase discontinuities for controlling light propagation. *Nano Lett.* **12**, 5750–5755 (2012).
16. G. Zheng, H. Mühlenbernd, M. Kenney, G. Li, T. Zentgraf, S. Zhang, Metasurface holograms reaching 80% efficiency. *Nat. Nanotechnol.* **10**, 308–312 (2015).
17. X. Zhang, Q. Xu, L. Xia, Y. Li, J. Gu, Z. Tian, C. Ouyang, J. Han, W. Zhang, Terahertz surface plasmonic waves: A review. *Adv. Photon.* **2**, 014001 (2020).
18. Q. Song, M. Odeh, J. Zúñiga-Pérez, B. Kanté, P. Genevet, Plasmonic topological metasurface by encircling an exceptional point. *Science* **373**, 1133–1137 (2021).
19. C. Spägele, M. Tamagnone, D. Kazakov, M. Ossiander, M. Piccardo, F. Capasso, Multifunctional wide-angle optics and lasing based on supercell metasurfaces. *Nat. Commun.* **12**, 3787 (2021).
20. R. C. Devlin, A. Ambrosio, N. A. Rubin, J. P. B. Mueller, F. Capasso, Arbitrary spin-to–orbital angular momentum conversion of light. *Science* **358**, 896–901 (2017).
21. Y. Yang, W. Wang, P. Moitra, I. I. Kravchenko, D. P. Briggs, J. Valentine, Dielectric meta-reflectarray for broadband linear polarization conversion and optical vortex generation. *Nano Lett.* **14**, 1394–1399 (2014).
22. Y. Zhang, J. Gao, X. Yang, Optical vortex transmutation with geometric metasurfaces of rotational symmetry breaking. *Adv. Optical Mater.* **7**, 1901152 (2019).
23. L. Huang, X. Chen, H. Mühlenbernd, H. Zhang, S. Chen, B. Bai, Q. Tan, G. Jin, K.-W. Cheah, C.-W. Qiu, J. Li, T. Zentgraf, S. Zhang, Three-dimensional optical holography using a plasmonic metasurface. *Nat. Commun.* **4**, 2808 (2013).
24. E. Maguid, I. Yulevich, M. Yannai, V. Kleiner, M. L. Brongersma, E. Hasman, Multifunctional interleaved geometric-phase dielectric metasurfaces. *Light Sci. Appl.* **6**, e17027 (2017).
25. R. Zhao, L. Huang, Y. Wang, Recent advances in multi-dimensional metasurfaces holographic technologies. *PhotoniX* **1**, 20 (2020).
26. X. Ni, A. V. Kildishev, V. M. Shalaev, Metasurface holograms for visible light. *Nat. Commun.* **4**, 2807 (2013).
27. Z.-L. Deng, J. Deng, X. Zhuang, S. Wang, K. Li, Y. Wang, Y. Chi, X. Ye, J. Xu, G. P. Wang, R. Zhao, X. Wang, Y. Cao, X. Cheng, G. Li, X. Li, Diatomic metasurface for vectorial holography. *Nano Lett.* **18**, 2885–2892 (2018).
28. H. Ren, W. Shao, Y. Li, F. Salim, M. Gu, Three-dimensional vectorial holography based on machine learning inverse design. *Sci. Adv.* **6**, eaaz4261 (2020).
29. R. Zhao, B. Sain, Q. Wei, C. Tang, X. Li, T. Weiss, L. Huang, Y. Wang, T. Zentgraf, Multichannel vectorial holographic display and encryption. *Light Sci. Appl.* **7**, 95 (2018).
30. A. Arbabi, Y. Horie, M. Bagheri, A. Faraon, Dielectric metasurfaces for complete control of phase and polarization with subwavelength spatial resolution and high transmission. *Nat. Nanotechnol.* **10**, 937–943 (2015).
31. D. Wen, J. J. Cadusch, J. Meng, K. B. Crozier, Vectorial holograms with spatially continuous polarization distributions. *Nano Lett.* **21**, 1735–1741 (2021).
32. Q. Song, X. Liu, C.-W. Qiu, P. Genevet, Vectorial metasurface holography. *Appl. Phys. Rev.* **9**, 011311 (2022).
33. H. Ren, Vectorial wavefront holography based on a polarisation-insensitive hologram. *J. Opt.* **24**, 064008 (2022).
34. C. Min, J. Liu, T. Lei, G. Si, Z. Xie, J. Lin, L. Du, X. Yuan, Plasmonic nano-slits assisted polarization selective detour phase meta-hologram. *Laser Photonics Rev.* **10**, 978–985 (2016).
35. J. Mun, S.-W. Moon, J. Rho, Multipole decomposition for interactions between structured optical fields and meta-atoms. *Opt. Express* **28**, 36756–36770 (2020).
36. H. Ahmed, H. Kim, Y. Zhang, Y. Intaravanne, J. Jang, J. Rho, S. Chen, X. Chen, Optical metasurfaces for generating and manipulating optical vortex beams. *Nanophotonics* **11**, 941–956 (2022).
37. G. Ruffato, M. Massari, F. Romanato, Multiplication and division of the orbital angular momentum of light with diffractive transformation optics. *Light Sci. Appl.* **8**, 113 (2019).

38. S. Rasouli, P. Amiri, V. V. Kotlyar, A. A. Kovalev, Characterization of a pair of superposed vortex beams having different winding numbers via diffraction from a quadratic curved-line grating. *J. Opt. Soc. Am. B.* **38**, 2267 (2021).
39. S. Zhang, P. Huo, W. Zhu, C. Zhang, P. Chen, M. Liu, L. Chen, H. J. Lezec, A. Agrawal, Y. Lu, T. Xu, Broadband detection of multiple spin and orbital angular momenta via dielectric metasurface. *Laser & Photonics Rev.* **14**, 2000062 (2020).
40. S. Fu, T. Wang, S. Zhang, C. Gao, Integrating 5 × 5 Dammann gratings to detect orbital angular momentum states of beams with the range of −24 to +24. *Appl. Optics* **55**, 1514–1517 (2016).
41. X. Zhang, L. Huang, R. Zhao, Q. Wei, X. Li, G. Geng, J. Li, X. Li, Y. Wang, S. Zhang, Multiplexed generation of generalized vortex beams with on-demand intensity profiles based on metasurfaces. *Laser Photonics Rev.* **16**, 2100451 (2022).

Acknowledgments
Funding: We acknowledge the funding provided by the National Key R&D Program of China (2021YFA1401200), the Beijing Outstanding Young Scientist Program (BJJWZYJH01201910007022), the National Natural Science Foundation of China (nos. U21A20140 and 92050117), the Beijing Municipal Science & Technology Commission, the Administrative Commission of Zhongguancun Science Park (Z211100004821009), the Fok Ying-Tong Education Foundation of China (no. 161009), and Hong Kong Research Council AoE grant no. 17309021. **Author contributions:** L.H. proposed the idea. X.Z. and R.Z. conducted pattern designs and numerical simulations. G.G., J.L., and Xiaowei Li fabricated the samples. X.Z., R.Z., H.Z., and Xin Li conducted the experiment measurements. L.H., X.Z., and S.Z. prepared the manuscript. L.H., S.Z., and Y.W. supervised the overall projects. All authors analyzed the data and discussed the results. **Competing interests:** The authors declare that they have no competing interests. **Data and materials availability:** All data needed to evaluate the conclusions in the paper are present in the paper and/or the Supplementary Materials.

Submitted 27 February 2022
Accepted 19 August 2022
Published 5 October 2022
10.1126/sciadv.abp8073

ScienceAdvances

Basis function approach for diffractive pattern generation with Dammann vortex metasurfaces

Xue ZhangLingling HuangRuizhe ZhaoHongqiang ZhouXin LiGuangzhou GengJunjie LiXiaowei LiYongtian WangShuang Zhang

Sci. Adv., 8 (40), eabp8073. • DOI: 10.1126/sciadv.abp8073

Science Advances (ISSN) is published by the American Association for the Advancement of Science. 1200 New York Avenue NW, Washington, DC 20005. The title *Science Advances* is a registered trademark of AAAS.